Sum-Frequency Spectroscopy of Surfactant Monolayers at the Oil−Water Interface

Mona Marie Knock,† Graham R. Bell, Elisabeth K. Hill, Hannah J. Turner, and Colin D. Bain*

Physical and Theoretical Chemistry Laboratory, University of Oxford, South Parks Road, Oxford OX1 3QZ, United Kingdom

Received: September 22, 2002; In Final Form: July 21, 2003

A new experimental arrangement is described for acquiring sum-frequency (SF) spectra from surfactants at the oil−water interface. The key features of this approach are the stabilization of a thin oil film between a sapphire prism and an aqueous phase and the use of total internal reflection to enhance the total signal and discriminate against signals from other interfaces in the system. With this new methodology, the first SF vibrational spectra of surfactant monolayers at an alkane−water interface were obtained. Surface tensiometry was used to characterize the monolayers further. The structure of monolayers of the cationic surfactant hexadecyltrimethylammonium bromide (CTAB) at the hexadecane−water interface was determined by sum-frequency spectroscopy (SFS) and compared with monolayers of CTAB at the air−water interface. At low concentrations, CTAB/hexadecane showed the expected features in the C−H stretching region, characteristic of a conformationally disordered monolayer. As the bulk concentration approached the critical micelle concentration, the spectra changed to one characteristic of a more ordered, upright conformation. Ellipsometric measurements supported this conclusion. This qualitative structural change is not observed in analogous monolayers at the air−water interface or CCl_4−water interface or in surfactant solutions in contact with a hydrophobic solid surface.

1. Introduction

Surfactants, whether natural or synthetic, are designed to aggregate at interfaces. Oil−water (o−w) interfaces in both natural and synthetic contexts are frequently modified by surfactants. Examples include the use of detergents to dissolve soil, oil−water emulsions for the cosmetic, food, petrochemical, and pharmaceutical industries,[1] and environmental groundwater remediation.[2] Though the consequences of surfactant adsorption at these interfaces are well-studied, there is little information available on the structure of surfactant monolayers at the oil−water interface—a critical step toward understanding the structure−function relationship between the surfactant monomer and its aggregates at the o−w interface.

In this paper, we present the first vibrational spectra of surfactant monolayers at the bulk o−w interface obtained by sum-frequency spectroscopy (SFS). SFS is a form of nonlinear vibrational spectroscopy that is sensitive only to molecules in noncentrosymmetric environments. In our experiments, the bulk oil and water phases are isotropic and therefore sum-frequency (SF) inactive. Surfactant molecules adsorbed at the interface, however, are in a noncentrosymmetric environment and give rise to SF spectra. The intensity and phase of peaks in SF spectra can be analyzed to obtain the polar orientation and tilt of molecules absorbed at interfaces. A unique feature of SFS, which is particularly useful for the study of surfactant molecules with their long hydrocarbon chains, is the sensitivity of the C−H stretching modes to the extent of conformational order in polymethylene chains. We have chosen as our model system the cationic surfactant hexadecyltrimethylammonium bromide ($CH_3(CH_2)_{15}N^+(CH_3)_3Br^-$, known as CTAB) at the interface between hexadecane and solutions of the surfactant in D_2O. CTAB has been widely studied at a variety of interfaces by our group[3−5] and others[6−8] and the adsorption behavior and sum-frequency spectroscopy of the surfactant is reasonably well-understood.

Structure of Paper. To set our work in context, we first provide a brief review of other techniques that have been used to study the o−w interface and of previous efforts to study liquid−liquid interfaces by nonlinear optical techniques. We then describe the design of a cell for the acquisition of SF spectra from the oil−water interface and discuss the various considerations that influenced the design. Next, we present SF spectra of the hexadecane−water interface for aqueous solutions of CTAB at different bulk concentrations and describe in some detail the correction procedures needed to normalize the raw spectra before they can be analyzed quantitatively or compared to SF spectra obtained at other interfaces. SF spectra are highly sensitive to changes in the surface excess, Γ. To separate the effect Γ from the effect of changes in the molecular structure at the interface, we obtained surface tension data for CTAB adsorbed at the oil−water interface by drop-shape analysis and determined the surface excess from a fit to the Szyszkowski equation. The SF spectra are then analyzed and compared with spectra of CTAB monolayers at the air−water (a−w) interface. Ellipsometric data are introduced to support the interpretation of the SF spectra.

Experimental Studies of the Oil−Water Interface. Surfactants at the o−w interface present particular difficulties for most surface-analytical techniques for several reasons. First, in the presence of adsorbed surfactants the surface tension, σ, of the o−w interface is greatly lowered, reaching a value of 4 mN m^{-1} at the critical micelle concentration (cmc) of CTAB. The

* Corresponding author. E-mail: colin.bain@chem.ox.ac.uk.
† Current address: Clorox Services Company; 7200 Johnson Drive; Pleasanton, CA 94588; e-mail: mona.knock@clorox.com.

10.1021/jp027047m CCC: $25.00 © 2003 American Chemical Society
Published on Web 09/09/2003

amplitude of thermally excited capillary waves scales as $\sigma^{-1/2}$ and the o−w interface is therefore much rougher than the a−w interface ($\sigma > 35$ mN m^{-1} for CTAB).[9] The effect of roughness is to wash out the fine structure of the interface in scattering experiments. Second, one of the bulk phases needs to be transparent to the incoming light or particle beam. Third, surfactants adsorbed at the interface need to be distinguished from those in the bulk phases. Finally, like most liquid interfaces, the o−w interface is highly sensitive to surface-active impurities.

Surface tensiometry has long been used to study the adsorption of surfactants at the o−w interface. A good recent study is that of Goebel and Lunkenheimer who examined the neat o−w interface with a modified ring method and pendant drop technique.[10] They measured the effect of impurities in the alkane phase on the o−w interfacial tension and achieved surface tension measurements to a high standard of interfacial purity. Even−odd effects from the length of the alkane chain were observed in the surface tension of the o−w interface. However, while surface tensiometry can provide thermodynamic parameters, such as surface excess or surface entropy, it provides no direct information on the structure of the interface on a molecular length scale.

Neutron scattering techniques, such as neutron reflectivity (NR) and small-angle neutron scattering (SANS), provide information on density distributions and adsorbed amounts at interfaces. The ability to vary the refractive index (and hence the "contrast" between the monolayer and the bulk phases) by deuterium substitution compensates for the inherently weak scattering of neutrons by matter. Interfacial roughness can dominate the results of NR, which also suffers from significant attenuation of the neutron beam during transmission through a liquid medium (especially one that contains hydrogen atoms). NR has been used to study polymer adsorption at a planar hexane−water interface.[11] SANS has been used to study adsorption of mixed surfactant layers at the o−w interface of a hexadecane-in-water emulsion.[12] Early NR studies of the liquid−liquid interface restricted one phase to volatile oils such as hexane which were condensed onto an aqueous liquid phase to form a thin film 1−4 μm in thickness, while the adsorbed layer was comprised of oil-insoluble molecules. A newer method employs a spin−freeze−thaw sequence to generate a thin oil layer between a silicon block and an aqueous solution. This method was used to study the adsorption of linear diblock copolymers at the hexadecane−water interface.[13]

X-ray reflectivity[14] has the advantage that X-ray transmission through the sample is less difficult than for neutron reflection and scattering. In hydrocarbon surfactants, however, the lack of refractive index contrast between the surfactant and the solvents limits its applicability to the oil−water interface. Grazing-incidence X-ray surface scattering was used to study a phospholipid monolayer at the hexadecane−water interface.[15] The study was hindered by scattering by the bulk alkane, by fluctuations in the height of the interface, and by the superposition of scattered X-rays from different boundaries within the interfacial layer (hexadecane/chain, chain/head, and head/water) though a basic description of a densely packed monolayer with all-trans chains determined. Schlossman et al. developed a method of flattening the hexane−water interface to reduce the interfacial roughness.[16] Solid−gas phase transitions in monolayers of partially fluorinated alcohols were later observed at the hexane−water interface.[17]

Optical techniques such as Brewster angle microscopy (BAM) and fluorescence have been used to study the o−w interface. BAM is sensitive to changes in density or orientation on a macroscopic length scale and is therefore of particular value in the study of domains of coexisting phases. Findenegg and co-workers used BAM to study temperature-induced phase transitions in monolayers of long-chain partially fluorinated alkanols at the hexane−water interface.[18] Fluorescence anisotropy measurements provide information on molecular reorientation. Most surfactants do not fluoresce, but fluorescent dyes doped into surfactant monolayers can be used to probe the structure of monolayers on the assumption that the probe does not interfere with the local structure and dynamics of the film. Fluorescence is also not surface-specific, so amphiphilic dyes, such as acridine orange, are needed. Wirth and co-workers studied monolayers of the anionic surfactant sodium dodecyl sulfate (SDS) containing acridine orange at the water−hexadecane interface to establish parallels between the behavior of the dye molecule in monolayers and micelles.[19] Attempts to repeat the experiment with a cationic surfactant, cetyltrimethylammonium chloride, failed because of charge repulsions between the cationic acridine orange dye and the surfactant. Fluorescence was also used to study the reorientation of acridine orange at an alcohol-modified hexadecane−water interface.[20] Gajraj and Ofoli have designed a total internal reflection fluorescence microscope (TIRFM) to study adsorption and interactions of labeled macromolecules (such as enzymatic proteins) at the oil−water interface.[21] Similarly, Radke et al. designed a total internal reflection fluorescence spectrometer (TIRFS) to follow dynamic adsorption and desorption of fluorescent macromolecules (labeled β-casein).[22]

Ellipsometry is a sensitive optical technique that measures the change in the polarization of light upon reflection from a planar interface.[23] It is convenient, nondestructive, and sensitive to variations in molecular adsorption at fluid interfaces. In contrast to surface tensiometry or neutron reflection, however, ellipsometry does not allow the unambiguous determination of the surface excess of surfactants at the o−w interface. Findenegg et al. studied the liquid−liquid interface between colloid-rich (colloidal liquid) and polymer-rich (colloidal gas) suspensions of silica colloids, poly(dimethylsiloxane) polymers, and cyclohexane, as well as weakly and strongly amphiphilic nonionic surfactants at various liquid−liquid interfaces.[24] Russev et al. studied the adsorption kinetics for β-casein at the a−w and o−w interfaces by ellipsometry[25] while Beaglehole and co-workers studied the amino acid tryptophan, the peptide tryptophan-leucine, and the protein bovine serum albumin at the buffered water−oleyl alcohol interface.[26] In general contrast to the behavior of monomeric surfactants, protein adsorption at the a−w and o−w interfaces was found to be very similar.

Second-order nonlinear optical effects are forbidden in centrosymmetric media and are therefore intrinsically surface-sensitive.[27] Second-harmonic generation (SHG) is a widely used nonlinear optical technique.[28] Analysis of polarization-dependent SHG measurements yields information on interfacial symmetry and the orientation and number density of an amphiphile within an adsorbed layer. From SHG, one can also infer the local dielectric properties of an interface[29] and, if the electronic spectrum is changed by protonation, determine the extent of ionization of adsorbed molecules and hence the surface pK_a.[30] SHG is a weak effect which relies on resonant enhancement of the molecular hyperpolarizability by electronic transitions. SHG is therefore restricted to the few surfactants with chromophores in accessible regions of the electromagnetic spectrum. Grubb et al. compared SHG from the surfactant sodium 1-dodecylnaphthalene 4-sulfonate (SDNS) at the a−w, decane−water, and CCl_4−water interfaces.[31] A significant difference in tilt (21°

vs 38°) for the naphthalene sulfonate moiety was found in saturated monolayers at the decane−water and carbon tetrachloride−water interfaces, indicating that the CCl_4–water interface is not necessarily a good model for the oil−water interface. A comparison of phenol, *p*-nitrophenol, and *p*-propylphenol at the a−w and hexane−water interfaces showed that the mean tilt was higher at the a−w than o−w interfaces, with the difference being greatest for phenols with a more hydrophilic substituent in the para position.[32] Interfacial liquid structure at the neat alkane−water interface has been studied by nonresonant total internal reflection SHG.[33] The alkane−water interfaces examined, particularly those with even-numbered alkane carbon chains, were highly ordered. The chain length had a significant effect on the degree of ordering in both the alkane and aqueous interfacial regions. The water−1,2-dichloroethane interface is popular for electrochemical studies. At this interface, SHG has been used to study an azobenzene surfactant and mixed monolayers of multiply charged polypeptides with charged surfactants.[34]

Most surfactants lack chromophores in the visible or near-UV, with the result that SHG is very weak and difficult to interpret in terms of chemical structure at the interface. A related nonlinear optical technique is infrared−visible sum-frequency generation (SFG), in which enhancement arises from vibrational transitions in resonance with the IR laser.[35] A visible laser is used to upconvert the IR laser into a readily detectable region of the spectrum. Since all surfactants have vibrations, sum-frequency spectroscopy (SFS) can be used to study any surfactant that forms an oriented film at an interface. Consequently, SFS has been widely used to study monolayers adsorbed at the solid−air,[36] solid−liquid[36a,37](where the solid is either hydrophilic or hydrophobic), and air−water[38] interfaces.

The major drawback of SFG compared to SHG for studying liquid−liquid interfaces is the opacity of liquid phases to the IR laser. For selected liquids, such as carbon tetrachloride, the window of transmission in the IR is wide and absorption of the IR laser by the bulk phase is inconsequential. Richmond and co-workers conducted several studies on surfactants at the CCl_4−water interface, which will be discussed in more detail later in this paper.[39] The neat alkane−water interface has also been studied by SFS in the O−H stretching region where the alkane is transparent.[40] Until now, studies of surfactants at the interface between water and hydrocarbon oils have been frustrated by the fact that both phases are significantly adsorbing in the regions of the mid-IR where the surfactant vibrations occur. We will show in this paper that SFS of surfactants at the o−w interface is possible if one uses deuterated oil, D_2O, and a protonated surfactant. Commercial deuterated alkanes and D_2O absorb quite strongly in the C−H stretching region, however, and thin liquid films have to be used.

It is worth mentioning briefly the body of literature on mixed monolayers of surfactants and oils at the a−w interface. When small drops of medium-chain alkanes ($n > 8$) are placed on the surface of an aqueous surfactant solution, the oil initially spreads quickly, resulting in an equilibrium between a mixed film of surfactant and oil coexisting with a macroscopic oil lens (or lenses)—a regime known as pseudopartial wetting.[41] These mixed monolayers are likely to have similarities to monolayers at the bulk o−w interface, but the absence of the bulk oil phase makes experimental measurements much easier. We have previously looked at mixed monolayers of alkanes and surfactants by SFS, ellipsometry, and surface tensiometry.[42] Two-dimensional solid−liquid-phase transitions were observed in the monolayer at temperatures that are very sensitive to the difference in chain length between the surfactant and the alkane. Thomas and co-workers carried out NR and surface tensiometry on mixed monolayers of dodecane with C_{14}TAB,[43] with C_{16}-TAB and C_{12}TAB,[44] and with pentaethylene glycol monododecyl ether.[45] Mixed monolayers of phospholipids with dodecane, hexadecane, or bicyclohexyl have been examined by ellipsometry and X-ray reflectivity.[46] The presence of oil in the mixed monolayer has a significant influence on the conformation of the surfactants. Through NR and surface tensiometry, Thomas and co-workers found that the surfactant chains are more extended and upright in the mixed monolayer than in the pure surfactant monolayer, as shown by the thickness of the alkyl chain region of the surfactant in the mixed monolayer. This increased thickness was accompanied by a slightly increased area per molecule of surfactant, which is in contrast to the usual decrease in monolayer thickness as the surface coverage decreases. In the presence of oil, Riegler and co-workers observed a reduction in tilt of the aliphatic chains of phospholipids, an increase in the thickness of the monolayer, and incorporation of alkane chains into the aliphatic chains of the phospholipid monolayer. Phase transition temperatures are not the same for monolayers at the a−w interface and at bulk liquid−liquid interfaces,[47] demonstrating that care must be taken when extrapolating from mixed monolayers to the bulk o−w interface.

Sum-Frequency Spectroscopy (SFS). In SFS, two pulsed laser beams are overlapped in space and time at an interface. One beam is usually in the visible (ω_{vis}) and the other in the mid-IR (ω_{IR}). Light is emitted at the sum-frequency ($\omega_{sum} = \omega_{vis} + \omega_{IR}$) with an intensity dependent on the second-order nonlinear susceptibility of the surface, $\boldsymbol{\chi}^{(2)}$, and the intensities of the incident laser beams, I_{vis} and I_{IR}:

$$I_{sum} \propto |\boldsymbol{\chi}^{(2)}|^2 I_{vis} I_{IR} \tag{1}$$

For protonated surfactants adsorbed at the interface between d_{34}-hexadecane and D_2O, the second-order nonlinear susceptibility in the C−H stretching region is dominated by contributions from a resonant term $\boldsymbol{\chi}^{(2)}_{R,\upsilon}$ that arises from the C−H stretching modes of adsorbed molecules. $\boldsymbol{\chi}^{(2)}_{R,\upsilon}$ is proportional to the number of molecules per unit area, N, and to the molecular hyperpolarizability, $\boldsymbol{\beta}$, averaged over all orientations of molecules at the interface.

$$\boldsymbol{\chi}^{(2)}_{R,\nu} = f\frac{N}{\epsilon_0}\langle \boldsymbol{\beta}_\upsilon \rangle \tag{2}$$

f relates the local electric field experienced by the molecules to the macroscopic electric field in the medium. $\boldsymbol{\chi}^{(2)}$ and $\boldsymbol{\beta}$ are third-rank tensors and change sign under inversion. Surfactant molecules in the bulk phase are randomly orientated and therefore contributions to $\boldsymbol{\chi}$ from molecules with one orientation are canceled by contributions from molecules with an opposing orientation. The orientational average over $\boldsymbol{\beta}$ thus vanishes in the bulk. Although the CTAB monolayers examined here are isotropic within the monolayer plane, they are asymmetric with respect to the surface normal. This anisotropy creates nonzero values of $\boldsymbol{\chi}^{(2)}$ which lead to SF emission. The SF signal strength is sensitive to the orientation of the molecules within the monolayer.

Away from a vibrational or electronic resonance, $\boldsymbol{\beta}$ is negligible. When the IR frequency nears the vibrational frequency, ω_υ, of an SF active mode in the molecule, $\boldsymbol{\beta}$ is enhanced. Within the electric dipole approximation, $\boldsymbol{\beta}$ can be expressed in terms of the Raman tensor, $\boldsymbol{\alpha}_\upsilon$, the IR transition

dipole moment μ_n, and the relaxation time, Γ^{-1}.

$$\boldsymbol{\beta}_v = \frac{\boldsymbol{\alpha}_{\iota}\mu_{v,n}}{2\hbar(\omega_v - \omega_{IR} - i\Gamma_v)} \quad (3)$$

Equation 3 shows that for a vibrational mode to be SF active, it must be both Raman and IR active. Centrosymmetric molecules obey the rule of mutual exclusion and are SF inactive. The middle of each C−C bond in an all-trans polymethylene chain is a local inversion center, with the result that the methylene modes of an all-trans chain separate into two sets of modes that are either Raman active or IR active, but not both. Consequently, the CH_2 vibrational modes of an all-trans chain are SF inactive. When a hydrocarbon chain contains gauche conformations, the C−C bond loses its local center of symmetry, and methylene modes are observed in the SF spectrum. As a result of this sensitivity to local symmetry within the hydrocarbon chain, SFS provides information on the conformation of the chain that is not readily available from other spectroscopic techniques. While there is not yet any satisfactory theory for the intensity of the methylene modes in SF spectra of hydrocarbon chains, the ratio of the line strengths of the symmetric CH_2 (d^+) and symmetric CH_3 (r^+) stretches (or vice versa) is an established empirical measure of conformational disorder.[48]

2. Materials and Methods

2.1. Materials. CTAB (99%, Aldrich) was recrystallized three times from 1:1 acetone/methanol. Ultrahigh purity water (Elga, UHQ) was used throughout. D_2O (99.9 atom %D, Aldrich) was used as received. Hexadecane (99%, Aldrich) was passed through activated alumina three times and tested negative for the presence of polar impurities.[49] d_{34}-hexadecane (99 atom %D) was obtained from CDN Isotopes, Quebec, Canada, and was used as received. The sapphire prisms used in the SF experiments were obtained from Crystran Crystals (BDH Advanced Materials Division, England). Decyltrichlorosilane (97%, Aldrich), dodecyltrichlorosilane (>99%, Fluka), decane (99+%, Aldrich), dodecane (99+%, Aldrich), and 1,1,1-trichloroethane (99%, Aldrich) were used as received. FTIR spectra of solutions of deuterated and normal hexadecane in CCl_4 (99.9+ % HPLC grade, Aldrich) were obtained on a Bio-Rad FTS6000 spectrometer.

Glassware was cleaned in an alkaline detergent (Decon 90) and rinsed thoroughly with ultrahigh purity water (Elga, UHQ). The effectiveness of the cleaning procedures has been established previously by surface tensiometry and ellipsometry.[4] The cleanliness of glassware was carefully monitored and periodically verified.

2.2. Surface Tensiometry. Surface tensiometry was performed by axisymmetric drop-shape analysis (IT Concept, Longessaigne, France) on digital images of a rising captive drop of hexadecane in water or in aqueous solutions of CTAB at 298 K. The shape of the drop is determined by a balance between buoyancy, which tries to distend the drop, and surface tension, which favors a spherical drop with a minimum surface area. The profile of the drop is computed by balancing the Laplace pressure, $p = \sigma\,(r_1^{-1} + r_2^{-1})$, where r_1 and r_2 are the local radii of curvature of the drop, against the hydrostatic pressure. Laplacian drops were analyzed to derive the interfacial tension. The precision of the readings obtained by this method is related to the Bond number

$$B = \frac{\Delta\rho g r^2}{\sigma} \quad (4)$$

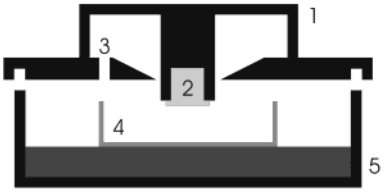

Figure 1. Cross section of oil−water sample cell used in SFS experiments. (1) adjustable height prism brace (2) hydrophobed sapphire prism (3) inlet for adjusting depth of CTAB solution (4) sample dish (5) adjustable height sample cell.

where $\Delta\rho$ is the density difference between the two phases, g the acceleration due to gravity, r the mean radius of the drop, and σ the interfacial tension. The volume of the drop was varied so that B fell in the range 0.01−0.2 for all values of the interfacial tension.

2.3. Sum−Frequency Spectroscopy. *2.3.1. Laser System.* The laser system has been described previously.[37] Briefly, a visible laser beam (s-polarized, 532 nm, 4 ns, 20 Hz, 2-mm diameter, 5 mJ pulse^{-1} for the o−w interface, 0.5 mJ pulse^{-1} for the sapphire−gold interface) was overlapped with a tunable infrared laser beam (p-polarized, 2800−3000 cm^{-1}, ∼1 ns, ∼1-mm diameter, 0.2−0.5 mJ pulse^{-1}) in a counter-propagating geometry at the oil−water interface. The sample chamber is described in detail in the following section. The SF signal originating from the o−w interface was emitted in a narrow beam. The blue SF light was directed through an edge filter (Omega Optical 452DF103) and a band-pass filter (Omega Optical 461.4DF20) to remove scattered green light and into a liquid nitrogen cooled CCD camera (Princeton Instruments) with a back-thinned chip. The angle of emission of the SF light is wavelength-dependent, so the SF signal tracks across the chip as the wavelength is scanned. No polarization-selecting element was placed in the SF beam because for an interface that is isotropic in the interfacial plane the polarization of the SF radiation is defined by the choice of input polarizations.

2.3.2. Sample Chamber. The sample chamber consists of a cylindrical metal lid and base in which sits a glass dish containing the surfactant solution beneath a thin oil film. The lid has one primary opening in which the removable prism holder is placed so that the base of the prism sits just above the level of the solution. A small hole in the lid allows the adjustment of the liquid level by addition of surfactant solution through a Pasteur pipet. The volume of the surfactant solution was ∼30 mL. Figure 1 illustrates a cross section of the sample chamber.

2.3.3. Alignment. SFS requires temporal and spatial overlap between the visible and infrared beams. This alignment is not trivial since the laser beams pass through several surfaces before intersecting at the oil−water interface. Optimization of the alignment on the o−w interface itself is difficult since only a small misalignment leads to vanishing of the SF signal. Initial alignment was therefore carried out with a sapphire prism identical to those used in the oil−water experiments but with the lower face coated with a thin layer of gold, which generates a strong nonresonant SF signal at all IR wavelengths. For the alignment measurements, the ppp-polarization combination was employed and the energy of the visible laser was reduced to 0.5 mJ pulse^{-1} to avoid ablation of the gold surface. The beam paths that gave the maximum signal from gold also gave the maximum signal from a surfactant monolayer at the oil−water interface.

2.3.4. Acquisition of SF Spectra. After alignment with the gold-coated prism, a ppp-polarized SF spectrum (where the

letters refer to the polarization of the SF, visible, IR fields in order) of gold was acquired in 2 cm^{-1} increments with 200 laser pulses per data point. The variation in SF signal from gold over the 3000−2800 cm^{-1} wavelength range arises principally from the variations in the IR power generated by the Raman shifter and was used subsequently to normalize the SF spectra from the o−w interface.

CTAB solutions were then prepared in D_2O at room temperature and placed in a clean 50-mm diameter glass dish inside the sample chamber. A drop of d_{34}-hexadecane was drawn over one surface of the sapphire prism with a tissue and a second drop was placed on the surface of the CTAB solution. The second drop normally broke up into a series of small lenses in equilibrium with a microscopically thin mixed monolayer of oil and CTAB. The lid containing the sapphire prism was placed on top of the sample chamber and the level of the CTAB solution was carefully raised by addition of CTAB solution until the surface of the solution made contact with the prism. Contact can be observed visually from the weakening of reflections of ambient light from the lower prism face. Incomplete wetting of the prism or penetration of the CTAB solution through the thin oil film is easily observed through perturbations in reflected ambient light. To confirm that the o−w interface was planar, the lasers were directed (at reduced power) into the sample chamber and a check made that the green and IR beams reflected from the o−w interface followed almost the same path as the incident beams. When present, a distorted, nonplanar o−w interface diverted the reflected beams from the path of the reflection from the prism−oil interface.

For SF spectra of CTAB solutions under hexadecane, the emitted SF signal is strongest at 2876 and 2938 cm^{-1}. These two peaks were located on the CCD image and used to determine the pixels of maximum signal at all other wavelengths. Binning selected pixels together at each wavelength minimizes the amount of background light and read-out noise, while still collecting all the SF photons. A computer program automatically tracked the sample spot during acquisition of a spectrum. Spectra were acquired at 2 cm^{-1} intervals between 2800 and 3000 cm^{-1} with 720 laser pulses for each data point (1 h in total per spectrum). The IR beam was then blocked and a background spectrum acquired at 10 cm^{-1} intervals. A linear fit to the background was subtracted from the original sample spectrum. The average IR pulse energies at 3000 and 2800 cm^{-1} were measured after each sample spectrum and subsequently used in the normalization procedure, which is described in detail in Section 4.1. All surfactant spectra were obtained with ssp-polarization. For this polarization, only one component of χ, χ_{yyz}, contributes to the SF signal.

2.3.5. Fitting SF Spectra. Each peak was characterized by a line strength S_v, a resonant frequency, ω_v, and a homogeneous line width, Γ_v, where

$$S_v(\omega_{IR}) = \frac{S_v}{\omega_v - \omega_{IR} - i\Gamma_v} \tag{5}$$

This complex function was convoluted with a Gaussian distribution of resonance frequencies of line width σ to account for inhomogeneous broadening. The resulting function, f_v, which is similar to a Voight function, was computed numerically for each resonance. Since the signal-to-noise ratio in these experiments was too low to separate the contributions of Γ and σ to the observed line width, Γ was fixed at a value of 2 cm^{-1} and only σ was allowed to vary. The nonresonant background from the oil−water interface was negligible. Each spectrum $S_{SF}(\omega_{IR})$ was then fitted with the function

$$S_{SF} = |\sum_v f_v(\omega_{IR})|^2 \tag{6}$$

2.3.6. Transmission of the Oil Film. After the acquisition of an SF spectrum of CTAB at the oil−water interface, the visible laser beam was blocked and the transmitted IR beam was monitored with a laser energy meter (Gentec Sun Em−1) in 2 cm^{-1} increments from 3000 to 2800 cm^{-1}. This process was repeated on different samples and the transmission spectra were averaged.

2.3.7. Coating of Sapphire Prism. A thin oil film between a clean sapphire prism and a solution of CTAB is only metastable and the surfactant solution was observed to break through the oil layer and preferentially wet the prism surface within 5−10 min. To prevent the surfactant solution from displacing the hexadecane film, the sapphire surface was modified with a hydrophobic, oleophilic alkylsilane coating. These coatings were not particularly durable and needed to be repeated on a regular basis, typically after one or two experiments.

Before sapphire prisms were recoated, the surfaces were washed with chloroform and UHQ water, to remove any oil or adsorbed surfactant, and then cleaned in hot "piranha solution" (30% of 30% H_2O_2, 70% concentrated H_2SO_4; *caution—piranha solution can react violently with organic materials*) for at least 30 min. After the piranha solution had cooled, the prisms were thoroughly rinsed with UHQ water. Prisms were left submerged under UHQ water until the time of their coating (typically a few hours).

Since no literature exists for silanization of a sapphire surface, various modifications of silanization procedures used for other substrates were explored. The silanization solution that worked best consisted of a mixture of 8 mL decane or dodecane with 8 mL 1,1,1-trichloroethane, to which approximately 5 mL of decyltrichlorosilane or dodecyltrichlorosilane, respectively, were added and well-mixed. Solutions were used immediately.

Prisms were removed from the UHQ water and briefly allowed to dry in air until surface water was no longer visible to the eye. (The microscopic water layer that remains encourages polymerization of the trichlorosilane at the prism surface. The absence of free −OH groups on the sapphire surface prevents covalent attachment of the polymerized silane monolayer to the surface, which probably accounts for the limited durability of these coatings compared to analogous films on silica.) The prisms were immersed in the silanization solution and rotated after 10 min of immersion so that all three polished surfaces had equal initial exposure to the reaction solution. The prisms were left to coat for 24 h or longer and were typically rotated once or twice more during that time. After 2 days, no discernible changes in the quality of the coating quality were observed.

The coating process was judged successful if the contact angle of water was >90° across the full area of a prism face. Particular care was paid to quality of the coating at the edges of the face, since it is here that breakthrough of the surfactant solution was most likely to occur. The quality of the coating was usually significantly better on one prism face than on the other two, suggesting that the cut of the sapphire prism influenced the silanization process. This preference was not investigated further.

3. Design of Cell for SFS of Oil−Water Interface

3.1. Transparency of Bulk Phases. The main challenge in obtaining SFS from the oil−water interface is delivering the IR radiation to the interface. One might think that absorption

by the bulk phase could easily be circumvented by studying protonated surfactants with deuterated alkanes or deuterated surfactants with normal alkanes. However, normal alkanes have an overtone in the C−D stretching region and commercial deuterated alkanes are only ca. 99% deuterated. Water and D_2O both have a significant adsorption cross section throughout the mid-IR. Consequently, the liquid phase through which the IR radiation passes can be at most 100 microns or so in thickness. Given that the alkane−water interface is bounded by a thin liquid film, there will be a second interface capable of generating SF light that will interfere with the SF signal of interest. Any design must therefore discriminate against this unwanted signal, either by physically blocking the signal or by ensuring that it is weak enough to be neglected.

Since water does not wet a pure alkane or a pure alkane water (except for pentane and shorter homologues, which are inconveniently volatile), the thin liquid phase needs to be confined by a solid surface. We chose to confine a thin film of hexadecane between a sapphire prism and a bulk aqueous surfactant solution. The problem of ensuring that the oil wets the prism is discussed later.

3.2. Total Internal Reflection. The SF signal from the oil−water interface is maximized when the visible and IR lasers are incident at the critical angle, θ_c, for total internal reflection (TIR). For green light, hexadecane ($n = 1.435$) has a higher refractive index than water ($n = 1.333$) so the conditions for TIR can be fulfilled if the visible laser is incident through the alkane at an angle above the critical angle, $\theta_c = 68.3°$. In the infrared, there are two ways of achieving TIR: protonated surfactants with deuterated oil and D_2O or deuterated surfactants with normal oil and H_2O. We designed a cell suitable for either combination but only report measurements on protonated surfactants in the C−H stretching region (2800−3000 cm^{-1}). Our laser system performs better between 2800 and 3000 cm^{-1} than between 2000 and 2200 cm^{-1}, C−H stretches are inherently more intense than C−D stretches, and there is a greater body of literature available on protonated surfactants than on deuterated surfactants to aid the interpretation of our results.

The two laser beams are introduced through an equilateral prism, rather than simply a window, to achieve the correct angle of incidence at the oil−water interface for TIR. Sapphire was chosen as window material since it is insoluble in water, robust, and transparent in the wavelength range of 3−5 microns where C−H and C−D stretches are found. The high refractive index of sapphire relative to water also makes alignment easier than would be the case with, for example, calcium fluoride. For sapphire, an angle of incidence of the visible laser $\theta_i = 20°$ at the air−prism interface is required for TIR at the critical angle for the hexadecane−water interface (see Figure 2). For an angle of incidence of the IR laser, $\theta_i = 21°$, at the air−prism interface, θ_i at the hexadecane−water interface varies from 63.3° at 2800 cm^{-1} to 64.2° at 3000 cm^{-1}. The critical angle meanwhile varies from 58.9° to 63.5° over the same wavelength range, so the IR is always incident above the critical angle. In our calculations, we have used values of 1.779, 1.771, and 1.689−1.702 for the refractive index of sapphire[50] at ω_{sum}, ω_{vis}, and ω_{IR} (2800−3000 cm^{-1}), respectively, and neglected the small birefringence of sapphire. The refractive index of the D_2O, n_t, varies from $1.199 + 0.0040i$ at 2800 cm^{-1} to $1.253 + 0.0014i$ at 3000 cm^{-1}.[51] For hexadecane, we have assumed a value of $n = 1.40$ at frequencies in the IR that are well away from vibrational resonances.

3.3. Fresnel Coefficients. Given that the laser beams pass through two interfaces, prism−oil and oil−water, it is important

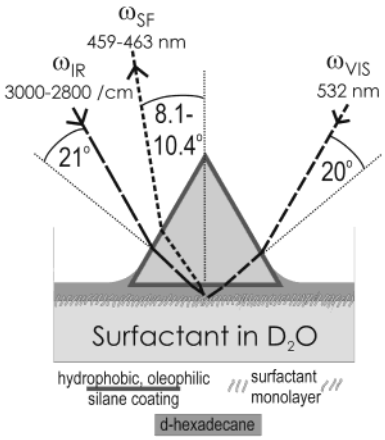

Figure 2. Optical geometry for total internal reflection at the oil−water interface. Angles for incident green and infrared light are shown with respect to the prism surface normals. Angles of SF emission are shown with respect to the surface normal of the optical table and interfacial plane.

to establish that the SF spectra arise from the oil−water interface rather than from the prism−oil interface. For the ssp-polarized spectra reported here, the SF signal, $S_{SF,s}$, (in photons per pulse) from a monolayer at the oil−water interface can be expressed as[52]

$$S_{SF,s} = \frac{2\epsilon_0 A\tau \cos\theta_{SF} I_{vis,s} I_{IR,p}}{\hbar\omega_{SF} c} |L^r_{SF,s,y} \chi^{(2)}_{yyz} K_{vis,s,y} K_{IR,p,z}|^2 \quad (7)$$

where K_{vis} and K_{IR} are Fresnel coefficients that relate the electric fields at the interface to the fields in the incident medium (oil) and L_{SF} relates the nonlinear polarization of the interface at the sum-frequency to the electric field of the SF beam emitted into the oil. In labeling the Fresnel factors, the subscript s denotes that the electric field E is perpendicular to the plane of incidence, the subscript p that E is parallel to the plane of incidence, and the superscript r that the field is evaluated in reflection rather than transmission. A Cartesian coordinate system is employed in which the $x-z$ plane contains the incident and reflected beams, z is normal to the interface, pointing upward from the water to the oil, and the oil−water interface lies in the $x-y$ plane. A and τ are the spatial and temporal overlap of the laser beams at the surface. θ_{SF} is the angle between the wavevector of the emitted SF light and the surface normal. An analogous expression can be written for the prism−oil interface.

We first consider the wavelength and angle dependence of each Fresnel factor for the oil−water interface. For nonabsorbing media, $|K_{vis,s,y}|$ always has the value 2 at the critical angle. Since E_y is continuous across the interface, the Fresnel coefficient has the same value whether evaluated in the D_2O, monolayer or the oil.

To compute $|K_{IR,p,z}|$, we first calculate the reflection coefficient, r_p, from[53]

$$r_p = \frac{n_t \cos\theta_i - n_i \cos\theta_t}{n_t \cos\theta_i + n_i \cos\theta_t} \quad (8)$$

where n_t is the complex refractive index of the D_2O and $\cos\theta_t$ is a complex number defined by $(1 - \sin^2\theta_t)^{1/2}$ and $\sin\theta_t$ is found from Snell's Law. θ_i is the (real) angle of incidence at the oil−water interface. $|K_{IR,p,z}|$ is then given by $|(1 + r_p)\sin\theta_i|$, where the electric field is evaluated in the oil. We assume that the chain region of the surfactant monolayer has the same

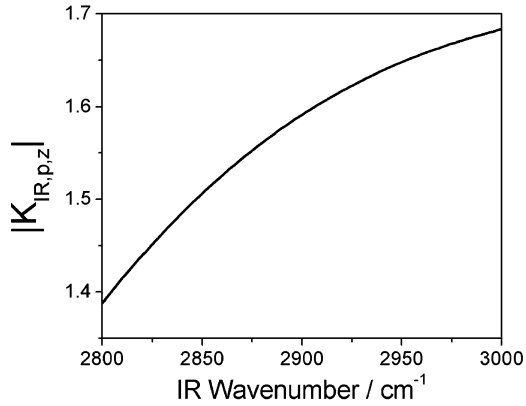

Figure 3. The variation in the Fresnel coefficient $|K_{IR,p,z}|$ with IR wavelength. $|K_{IR,p,z}|$ is the ratio of the *z*-component of the electric field at the oil−water interface to the incident field in a p-polarized beam in the oil.

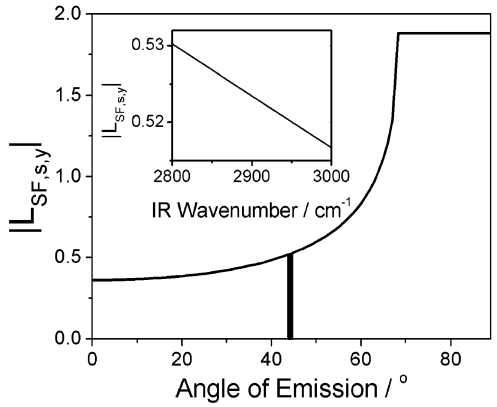

Figure 4. Variation in $|L_{SF,s,y}|$ with angle of emission at the oil−water interface. $|L_{SF,s,y}|$ relates the *y*-component of nonlinear polarization of the oil−water interface at the sum-frequency to the electric field of the s-polarized SF beam emitted into the oil. The shaded block indicates the range of angles arising in these experiments. The inset graph shows the small variation in $|L_{SF,s,y}|$ as the IR wavelength is scanned.

dielectric properties as the oil, so continuity of ϵE_z yields the same expression for $|K_{IR,p,z}|$ in the monolayer. The variation in $|K_{IR,p,z}|$ with IR wavelength is shown in Figure 3.

The variation in $|L^r_{SF,s,y}|$ with wavelength arises from the fact that the angle of emission of the SF beam varies with wavelength as a result of conservation of photon momentum, $\hbar k$, parallel to the surface: $k_{sum} \sin \theta_{sum} = k_{vis} \sin \theta_{vis} - k_{IR} \sin \theta_{IR}$. The effect of the dispersion in the refractive indices over the small range of wavelengths (459−463 nm) is insignificant. Figure 4 shows the variation in $|L^r_{SF,s,y}|$ with angle of emission: arrows on the graph indicate the range of angles of emission in this experiment. The inset to Figure 4 shows $|L^r_{SF,s,y}|$ as a function of incident IR wavenumber for our chosen geometry.

The angles of incidence at the o−w interface are chosen to maximize the electric fields of the incident lasers at that interface. Plots of the three Fresnel coefficients as a function of angle of incidence at the prism−oil interface are shown in Figure 5, with the experimental angles indicated by arrows. At this interface, the electric fields are well below their maximum values. To demonstrate that the cell design is indeed specific to the oil−water interface, we can compare the geometric factors affecting the sum-frequency signal. From eq 7

$$I_{SF} \propto \cos \theta_{SF} |L^r_{SF} K_{vis} K_{IR}|^2 \tag{9}$$

The ratio of these geometric factors for the oil/water to the prism/oil interface at 2900 cm^{-1} is

$$\frac{I_{oil-water}}{I_{prism-oil}} = \frac{\cos 44°}{\cos 34°} \times \left(\frac{0.522}{0.353}\right)^2 \times \left(\frac{2}{1}\right)^2 \times \left(\frac{1.588}{\sin 64°}\right)^2 = 24$$

Thus, TIR at the oil−water interface is expected to amplify the SF signal such that it overwhelms any SF signals arising from the prism−oil interface. This prediction was confirmed experimentally, as is shown later in Figure 10.

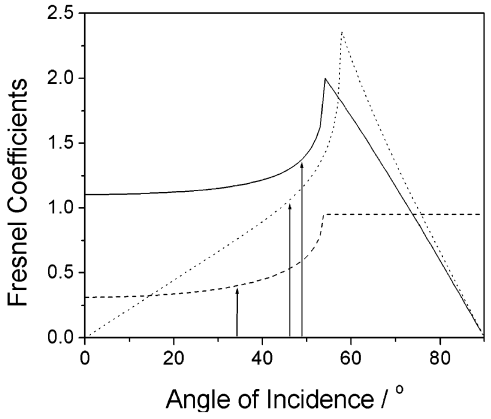

Figure 5. Fresnel coefficients calculated for the prism−oil interface, relating the electric fields at the prism−oil interface to the electric fields in the prism: solid line, $|K_{vis,s,y}|$; dotted line, $|K_{IR,p,z}|$ at 2900 cm^{-1}; dashed line, $|L_{SF,s,y}|$. The *x*-axis shows the angle of incidence at the prism−oil interface. The arrows indicate the angles actually employed in these experiments. Angles were chosen for total internal reflection (TIR) at the oil−water interface rather than the prism−oil interface, hence, the distance of the arrows from the peak values for TIR at the prism−oil interface shown in this figure. The ordinate scale does not directly give the values of the Fresnel coefficients in eq 9 since the interfacial fields in this figure are referenced, by convention, to incident fields in the prism.

We have employed a counter-propagating geometry with respect to the visible and IR beams. Theoretically, we could obtain even greater SF signal from the oil−water interface by choosing a co-propagating geometry in which the angle of emission of the SF beam was closer to the critical angle (Figure 4). A co-propagating geometry would be more difficult experimentally given the design of our optical bench and, as the spectra themselves demonstrate, the counter-propagating geometry produces ample signal from the surfactants at the o−w interface.

3.4. Stability of the Oil Film. Maintaining the stability of a thin film of oil between the prism and the surfactant solution is not trivial; after all, surfactants are designed to remove oil from solid surfaces. For a thermodynamically stable film, we require that, for all concentrations of surfactant, the interfacial tensions satisfy

$$\sigma_{sw} > \sigma_{so} + \sigma_{ow} \tag{10}$$

where s, w, and o refer to the sapphire, aqueous solution, and oil, respectively. If eq 10 is not satisfied, there is a tendency for the water to break through the thin oil film and cause the oil to retract from the prism. Equation 10 can be rewritten in terms of the contact angles (in air) of the oil (θ_o) and the surfactant solution (θ_w) on the prism:

$$\sigma_o \cos \theta_o - \sigma_w \cos \theta_w > \sigma_{ow} \tag{11}$$

where σ_o and σ_w are the surface tensions of oil and the aqueous solution, respectively. To satisfy this inequality, we seek to minimize θ_o and maximize θ_w. Functionalizing the prism with a methyl-terminated self-assembled monolayer (SAM) is one

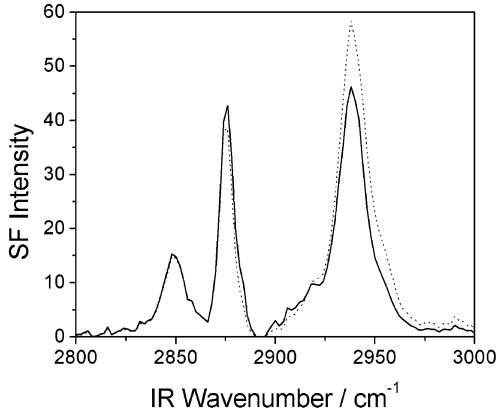

Figure 6. SF spectrum of CTAB monolayer at the oil−water interface, before (dotted line) and after (solid line) normalization. Units for the raw spectrum are in photons per pulse; units after normalization are arbitrary. The dc offset of the detector and any background light from the green laser have been subtracted.

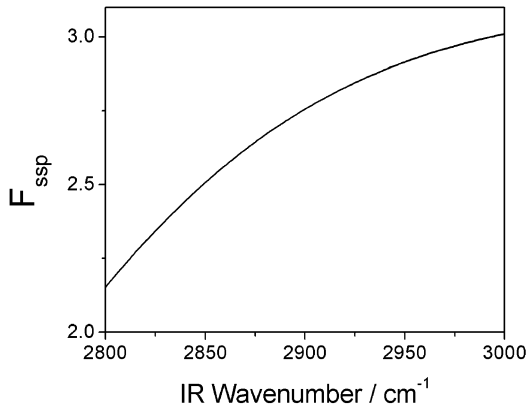

Figure 7. F_{ssp} as a function of IR wavenumber. The combined effect of the Fresnel coefficients at the oil−water interface on the SF spectrum is represented by a term $F_{ssp} = (L^{r}_{SF,s,y})^2 (K_{vis,s,y})^2 (K_{IR,p,z})^2$.

possibility, but substitution of literature values for $\sigma_o = 27$ mN m^{-1}, $\theta_o = 45°$, $\sigma_w^0 = 72$ mN m^{-1}, $\theta_w^0 = 115°$, $\sigma_{ow}^0 = 53$ mNm^{-1} shows that this inequality is not satisfied for pure water (indicated by the superscript 0). Introducing chain disorder into a SAM has a much greater effect on the oleophobicity than the hydrophobicity.[54] If a disordered monolayer reduces θ_o to zero while retaining a value of $\theta_w^0 > 111°$, then the inequality in eq 9 is satisfied, at least for pure water. (Experimentally, we found that it was most difficult to maintain a wetting film of hexadecane on the prism with pure water.) In practice, the requirements on the contact angles should not be as severe as this, since contact angle hysteresis will work in favor of the prism remaining wet by oil. We therefore sought a protocol for silanizing the sapphire prism to make it oleophilic yet hydrophobic. The procedure we adopted is described in section 2.3.6, but the success of the coating process was mixed and the durability of the coating was limited: improved coating procedures would be desirable.

4. Results

4.1. Normalization of SF Spectra. Figure 6 shows a raw SF spectrum of a solution of 0.6 mM CTAB at the oil−water interface, together with the spectrum after correction for all the wavelength-dependent factors that affect the intensity of the SF spectrum but are unrelated to the nonlinear susceptibility of the interface. Careful normalization is required before quantitative analysis and therefore we set out the various steps in detail.

4.1.1. Fresnel Coefficients. For ssp-polarized spectra, the SF signal is given by eq 7. The Fresnel coefficients $K_{vis,s,y}$, $K_{IR,p,z}$, and $L^{r}_{SF,s,y}$ and their wavelength dependence are discussed in section 3.3. In computing $K_{IR,p,z}$ we have assumed a constant value of $\epsilon_{monolayer} = \epsilon_{oil} = 1.96$. We note that $\epsilon_{monolayer}$ may vary significantly over the wavelength of interest because of the adsorption by the C−H stretching modes in the surfactant, but it is difficult to correct quantitatively for the dispersion in $\epsilon_{monolayer}$. The combined effect of the Fresnel coefficients at the oil−water interface on the SF spectrum is represented by a term $F_{ssp} = (L^{r}_{SF,s,y})^2 (K_{vis,s,y})^2 (K_{IR,p,z})^2$, which is plotted in Figure 7.

4.1.2. Laser Output. The performance of the laser system makes a major contribution to the variation in SF intensity with IR wavelength. The output power of the Raman cell decreases with increasing wavelength and also contains small dips because of traces of water vapor in the Raman cell. We quantified this variation by acquiring an SF spectrum from a sapphire prism in which the face normally in contact with the oil had been coated with a thin film of gold. Spectra of gold were taken at intervals during the experiments and the average spectrum is shown in Figure 8 a. The small loss of blue SF light because of reflection within the prism is present in the SF spectrum of gold and is thus accounted for as well. Variations in transmitted SF power with wavelength for the IR beam at the entry face of the prism and at the prism−oil interface are negligible.

We took into account day-to-day fluctuations in the average IR pulse energy by measuring the IR energy at 3000 and 2800 cm^{-1} before each spectrum and dividing the SF spectrum by the mean pulse energy. The pulse energy in the visible did not vary significantly.

4.1.3. Absorption of IR by Oil. The most significant correction arises from the small percentage (ca. 2%) of C−H bonds in the sample of deuterated hexadecane. Isolated CHD groups absorb IR light at 2892 cm^{-1} while CHD_2 groups have two absorptions at 2940 and 2926 cm^{-1}, depending on whether the C−H bond is in or out of the plane of the carbon skeleton, respectively.[55] The significance of these absorptions is seen in Figure 8b, which shows the intensity of the IR beam after reflection from the oil−water interface. The variation observed in Figure 8b with wavelength has three contributions: (i) the wavelength dependence of the output power of the Raman cell; (ii) absorption of IR in the evanescent wave in the D_2O; (iii) absorption by C−H bonds during two passages of the IR beam through the oil. The variation in the incident IR power can be removed through division of the spectrum in Figure 8b by the spectrum in Figure 8a, the result of which is shown in Figure 8c. The absorption by D_2O in the evanescent field is found by computing the reflectivity, $\mathscr{R}_{ow} = |r_p|^2$ (eq 8), of the oil−water interface, which is equal to 0.91 at 2900 cm^{-1} and approximately independent of wavelength. The lack of wavelength dependence is at first sight surprising, but it arises from the cancellation of two effects. As the wavelength increases, the imaginary part of the refractive index increases but at the same time the penetration depth of the evanescent wave decreases since the difference between the angle of incidence and the critical angle increases with increasing wavelength. The constancy of $\mathscr{R}_{ow}$ means that absorption of IR by D_2O can be ignored for the purpose of determining the intrinsic absorption of the oil film from the reflection spectra of the o−w interface. The SF signal is determined by the IR intensity after only one pass through the oil film and therefore to correct for absorption by C−H bonds in the oil, we need to take the square root of the transmission spectrum 8c, which is shown in Figure 8d. For comparison, the IR absorption spectrum of a dilute solution of d_{34}-hexadecane in CCl_4 is shown in Figure 8e.

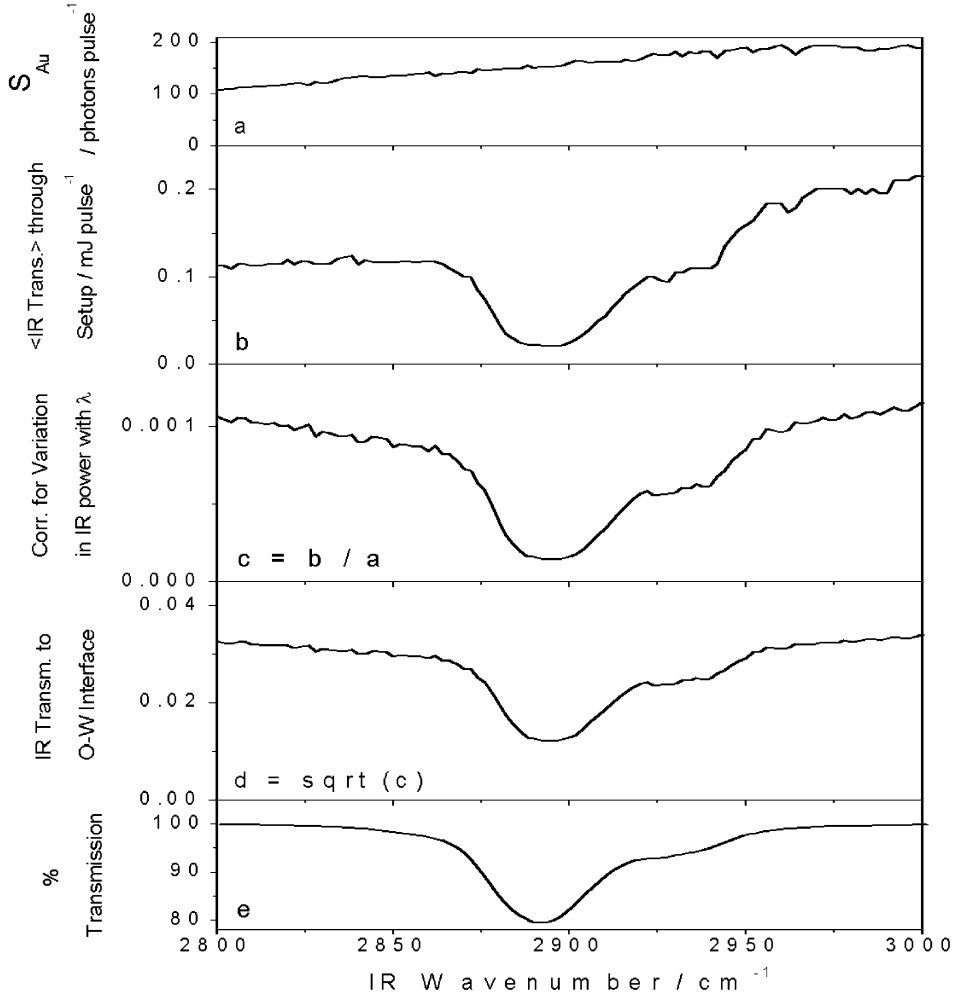

Figure 8. (a) Average SF spectrum (S_{Au}) of gold (ppp-polarization) in photons per pulse; (b) IR transmission through oil−water setup in mJ per pulse; (c) IR transmission corrected for variation in IR power with wavelength: $c = b/a$; (d) IR transmission to oil−water interface: $d = \sqrt{c}$; (e) % transmission of 8.7×10^{-3} M d_{34}-hexadecane in CCl_4 (path length = 0.95 cm).

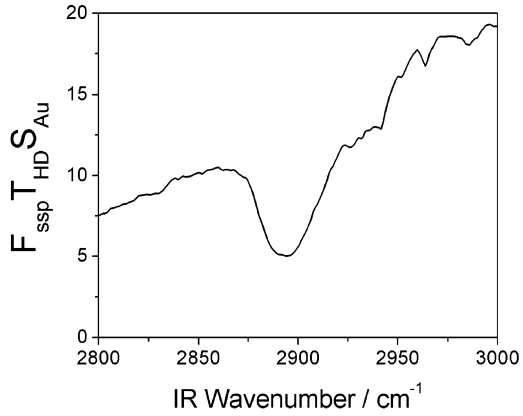

Figure 9. The composite correction factor for normalization of SF spectra at the oil−water interface. This factor accounts for Fresnel coefficients, reflection losses in the prism, variations in laser power, and absorption by the oil. To normalize an SF spectrum, this factor is multiplied by the average IR power associated with that spectrum, and then the product is divided into the spectrum.

The composite correction factor, taking into account Fresnel coefficients, reflection losses in the prism, variations in laser power, and absorption by the oil, is shown in Figure 9. The result of applying this correction to a sample SF spectrum of a CTAB monolayer is shown in Figure 6.

4.2. Thickness of the Oil Layer. We determined the thickness of the oil film by comparing the IR transmission spectrum of the oil film, described in section 2.3.5 and shown in Figure 8d, with reference spectra of the oil. FTIR spectra of solutions of deuterated and normal hexadecane in CCl_4 (4.0, 4.2, 8.4, and 8.7×10^{-3} M for d_{34}-hexadecane; 2.0×10^{-3} M for *h*-hexadecane) were obtained. A transmission spectrum of 8.7×10^{-3} M d_{34}-hexadecane in CCl_4 is shown in Figure 8e. The molar absorption coefficient, $\epsilon = 10.8 \pm 0.1$ dm^3 mol^{-1} cm^{-1}, at the peak maximum of the CHD stretch (2891 cm^{-1}) arising from residual hydrogen in the deuterated hexadecane was determined from the Beer−Lambert law. By comparing the integrated molar absorption coefficient over the C−H stretching region in deuterated and normal hexadecane, we estimate that the residual level of hydrogen in the d_{34}-hexadecane is 3%, compared with the nominal value of <1%.

The transmission spectrum of the IR laser through the thin film of deuterated hexadecane between the prism and water (Figure 8d) yields an absorbance of 0.43 at 2891 cm^{-1}, relative to a region of the spectrum where the oil does not absorb. Using the value of ϵ determined above and the neat concentration of 3.40 mol dm^{-3} of hexadecane, we calculate a path length, l, for the IR laser in the oil of $l = d/\cos q = 117$ μm, where d is the mean thickness of the oil layer and q the angle that the IR beam makes with the surface normal in the oil. Since $q \sim 64°$, $d \sim 50$ μm. This value agrees well with the average film thickness estimated from the volume of deuterated hexadecane applied to the surfaces of the prism and surfactant solution.

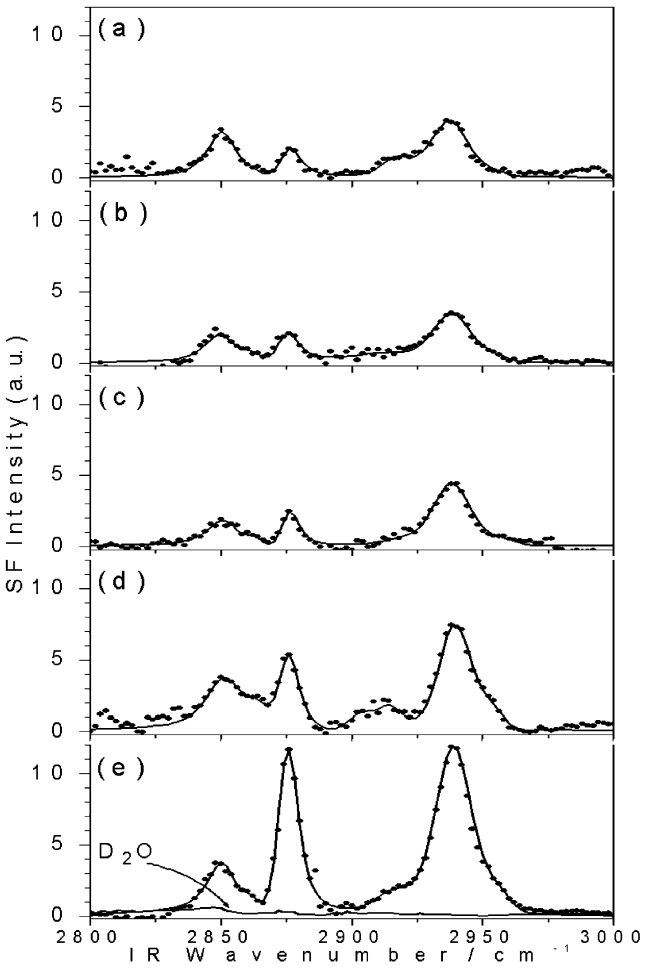

Figure 10. SF spectra of CTAB at the oil−water interface (ssp-polarization). From top to bottom: (a) 0.05 mM CTAB, (b) 0.1 mM CTAB, (c) 0.3 mM CTAB, (d) 0.5 mM CTAB, (e) 0.6 mM CTAB compared with pure D_2O.

For deuterated oils of commercial purity (ca. 98%), the practical upper limit for the thickness of the oil film is thus ca. 100 μm. For normal protonated surfactants and oils, the limiting film thickness would be only about 2 μm.

4.3. SF Spectrum of a CTAB Monolayer at the Oil−Water Interface. Figure 10e shows an overlay of SF spectra acquired from the interface between deuterated hexadecane and both 0.6 mM CTAB and pure D_2O. The solid line through the CTAB spectrum is a best fit to eq 6. The solid line through the spectrum of pure water connects data points only. The faint peaks discernible in the spectrum of the pure oil−water interface probably arise from the alkylsilane coating on the prism. The weakness of these peaks confirms the prediction that SF signals from the oil−water interface in the TIR geometry are much stronger than those from the prism−oil interface (Section 3.3). The strength of the SF field from the prism−oil interface is independent of the concentration of surfactant in the aqueous solution. The contribution of the alkylsilane to the SF spectra reported here will therefore be negligible.

The assignment of peaks in the SF spectra of surfactant monolayers has been discussed in detail previously.[48] ssp-Polarized CTAB spectra have three prominent peaks: the d^+ symmetric CH_2 stretch at 2852 cm^{-1}, the r^+ symmetric CH_3 stretch at 2876 cm^{-1}, and the $r_{FR}{}^+$ mode at 2938 cm^{-1}, which arises from a Fermi resonance of the symmetric CH_3 stretch with the overtone of the CH_3 bend. Of these peaks, the first two provide structural information about the monolayer. The

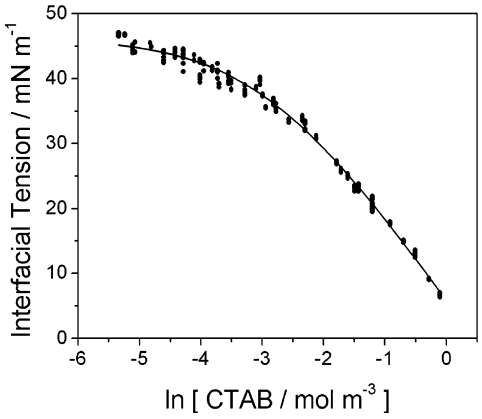

Figure 11. Interfacial tension of CTAB at the oil−water interface as a function of bulk CTAB concentration. Experimental data points (dots) fit to Szyszkowski eq (line).

d^+ mode is indicative of conformational disorder within the monolayer. For highly ordered monolayers with few gauche defects, the d^+ mode is very weak. As disorder increases, $\langle\beta_{yyz}\rangle$ increases because of the presence of gauche defects. For a highly disordered monolayer, one might expect $\langle\beta_{yyz}\rangle$ to decrease again because of cancellation between opposing conformations within the randomly orientated chains.

The line strength of the r^+ mode is dependent on the tilt of the terminal methyl group. In an ssp-spectrum, the component of the hyperpolarizability responsible for the signal from this mode is expressed in molecular coordinates as

$$\langle\beta_{yyz}\rangle = \frac{\beta_{ccc}}{8}\{\langle\cos\theta\rangle(1+7r) + \langle\cos 3\theta\rangle(r-1)\} \quad (12)$$

where $r = \beta_{aac}/\beta_{ccc}$ and θ is the angle between the surface normal (z) and the C_3-axis of the terminally methyl group (the *c*-axis). As the first bracketed term dominates in eq 12, $\langle\beta_{yyz}\rangle$ is proportional to $\langle\cos\theta\rangle$, to a good approximation.

4.4. Effect of Concentration on SF Spectra. The effect of concentration on the SF spectra of CTAB monolayers at the oil−water interface is shown in Figure 10 for five concentrations of CTAB ranging from 0.05 mM to 0.6 mM. The concentration of CTAB was kept below the critical micelle concentration (cmc = 0.92 mM) to prevent solubilization of the oil within micelles. In previous experiments on CTAB monolayers at the air−water interface, we found little difference between the spectrum of a monolayer formed from a 0.6 mM solution and from a solution at the cmc.[4]

In constructing a microscopic picture of the adsorbed surfactant film, it is more useful to correlate the spectra with the surface concentration of the surfactant, Γ, than the bulk concentration. It is difficult to determine Γ from SFS spectra alone, with any accuracy, so we determined Γ independently by drop-shape analysis. Figure 11 shows surface tension measurements on drops of hexadecane in CTAB solutions in the concentrations range 0.0048−1.2 mM. The data were fit to the Szyszkowski equation[56]

$$\sigma = \sigma_0 - 2RT\Gamma_m\ln(1 + K_L c) \quad (13)$$

At 298 K, the maximum surface excess, Γ_m, was $2.8 \pm 0.1 \times 10^{-6}$ mol m^{-2} with $K_L = 18 \pm 1$ m^3 mol^{-1}. The Szyszkowski equation is consistent with the Langmuir adsorption isotherm, $\Gamma = \Gamma_m\,[K_L c/(1 + K_L c)]$, from which Γ can be obtained at all other concentrations. The fit is poor at low concentrations of CTAB, reflecting the fact that the Szyszkowski equation does

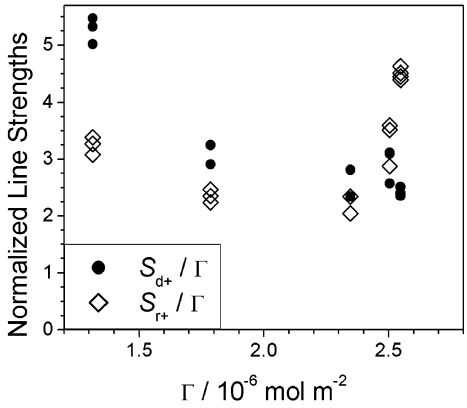

Figure 12. Line strengths of the d^+ mode (filled circles) and r^+ mode (unfilled diamonds) in SF spectra of CTAB at the oil−water interface. Line strengths were normalized for area per molecule.

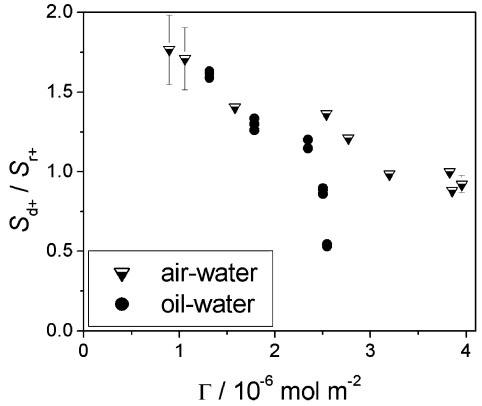

Figure 13. Ratio of line strengths of the d^+ and r^+ modes, S_{d+}/S_{r+}, as a function of surface excess, Γ, of CTAB at the oil−water interface (circles) and air−water interface (triangles).

not take account of electrostatic interactions, but is quite good at the concentrations employed in the SFS experiments, for which Γ varies from 1.3 to 2.6 × 10^{-6} mol m^{-2}.

5. Discussion

5.1. Effect of Area per Molecule on the SF Spectra of CTAB Monolayers. To interpret SF line strengths, *S*, in terms of changes in the conformation or orientation of molecules within the monolayer, we first must correct for the area per molecule, *A*. Since $S \propto \Gamma$, multiplication of *S* by $A = \Gamma^{-1}$ normalizes the line strength on a per molecule basis. Figure 12 depicts the variation in the normalized line strengths of the d^+ and r^+ modes with Γ. The normalized intensity of the d^+ mode decreases as Γ increases, indicating an increase in trans segments in the hydrocarbon chain as the density of CTAB molecules at the interface increases. The r^+ mode tells us about the orientation of the terminal methyl group, which is a reflection of the average tilt of the hydrocarbon chains within the monolayer. The most notable feature is the sharp increase in the r^+ line strength as the bulk concentration approaches the cmc, suggesting a transition to a much more upright configuration in the chains.

Interpretation of the normalized line strengths is susceptible to systematic errors in the determination of *A*. The ratio S_{d+}/S_{r+} is independent of *A*. This ratio has been correlated empirically to the degree of conformational disorder in surfactant monolayers.[39d,48,57] Figure 13 shows that S_{d+}/S_{r+} decreases with increasing surface excess, with a particularly sharp decrease as Γ approaches its limiting value at high surface coverage. This

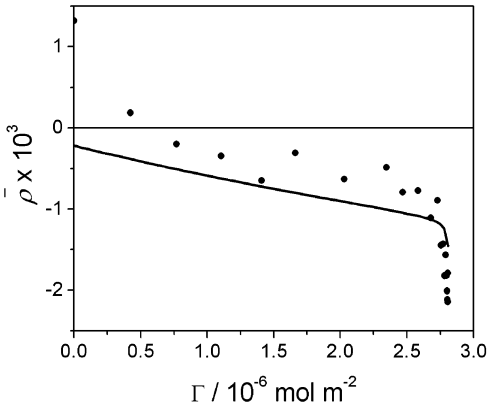

Figure 14. Coefficient of ellipticity, $\bar{\rho}$, for a CTAB monolayer at the oil−water interface, as a function of surface excess. Experimental values are indicated by dots; the predicted model is shown by a solid line. Ellipsometry was carried out with a picometer ellipsometer (Beaglehole Instruments, Wellington, New Zealand), which employed birefringence modulation at 50 kHz. The light source was a He−Ne laser at 632.8 nm. All measurements were carried out at the Brewster angle.

analysis supports the picture of a more upright, ordered conformation at higher surface coverages.

The sharp increase in the normalized value of S_{r+} and the decrease in the ratio of S_{d+}/S_{r+} over a very small change in the surface excess is unexpected, and we have looked for supporting evidence for a structural change in other measurements. Such evidence is to be found by ellipsometry. Details of the procedure may be found elsewhere,[4] but the results of measurements on CTAB at the hexadecane−water interface are shown in Figure 14. The ordinate is the coefficient of ellipticity, $\bar{\rho}$, which is defined as the imaginary part of the ratio r_p/r_s at the Brewster angle, where r_p and r_s are the reflection coefficients for s- and p-polarized light, respectively. The abscissa is the surface excess, derived from independent measurements of the interfacial tension. The predicted values of $\bar{\rho}$, calculated on the assumption that the hydrocarbon part of the surfactant chain has identical optical properties to hexadecane (see Appendix), is shown by a solid line. We see that the agreement between the experimental and predicted trends in $\bar{\rho}$ is quite good, except for the pure hexadecane−water interface (which we will not discuss here) and for values of Γ near the limiting surface excess, where there is a steep fall in the $\bar{\rho}$ against Γ plot. To explain this discrepancy, we need to look at the contribution of the hydrophobic chains of the surfactant to $\bar{\rho}$. For a monolayer with uniaxial symmetry, the optical properties of the chain region of the monolayer are characterized by two dielectric constants, ϵ_e, perpendicular to the surface, and ϵ_o, in the plane of the surface. $\bar{\rho}$ is given by[58]

$$\bar{\rho} = \frac{\pi}{\lambda} \frac{\sqrt{(\epsilon_1 + \epsilon_2)}}{\epsilon_1 - \epsilon_2} \eta \qquad (14)$$

where ϵ_1 and ϵ_2 are the dielectric constants of the alkane and water, respectively, λ is the wavelength of light, and the ellipsometric thickness η is given by

$$\eta = \frac{(\epsilon_e - \epsilon_1)(\epsilon_e - \epsilon_2)}{\epsilon_e} d + (\epsilon_o - \epsilon_e) d \qquad (15)$$

where *d* is the thickness of the chain region. We see that for $\epsilon_e = \epsilon_o = \epsilon_1$, the contribution to η from the hydrocarbon chains vanishes. One might expect that at high surface coverages of CTAB, the chain region would become denser than neat hexadecane, but this would lead to $\epsilon_e > \epsilon_1$ and a positive

contribution to η and $\bar{\rho}$. If, however, the chains adopt a preferred orientation along the surface normal, which is the implication of the SFS data, then $\epsilon_e > \epsilon_o$ and there is a negative contribution to $\bar{\rho}$, in agreement with the observed ellipsometric data. An anisotropy $\Delta\epsilon = \epsilon_e - \epsilon_o \approx 0.03$ would be sufficient to explain the experimental observations. For comparison, $\Delta\epsilon \approx 0.17$ in a monolayer of vertically oriented hydrocarbon chains in a hexagonal phase.[59]

5.2. Comparison with Monolayers at Other Interfaces. *5.2.1. CTAB at the Oil−Water and Air−Water Interfaces.* In comparison with the o−w interface, there is a wealth of information about the structure of surfactant monolayers at the a−w interface, principally from neutron reflection, X-ray reflection, FTIR, and SFS.[60] CTAB monolayers at the a−w interface have been studied in detail by NR[61] and by SFS.[4] The first point of comparison is that the maximum surface excess of CTAB is significantly higher at the a−w interface ($\Gamma = 3.9 \times 10^{-6}$ mol m^{-2}) than at the o−w interface ($\Gamma = 2.9 \times 10^{-6}$ mol m^{-2}). This difference can be ascribed to the mixing of oil and surfactant chains in the monolayer. In Figure 13, we compare the ratio S_{d+}/S_{r+} for CTAB monolayers at the o−w and a−w interfaces. At low surface coverages, the degree of conformational order is similar, but at higher surface coverages the ratio S_{d+}/S_{r+} is much lower at the o−w interface than for a comparable a−w interface. A priori, this difference could be ascribed either to a smaller number of gauche defects at the o−w interface or to a more upright configuration (and hence a larger value of $\langle\cos\theta\rangle$); in practice, a combination of both effects is likely. We note that for monolayers of CTAB at the air−water interface, $\bar{\rho}$ is a linear function of the surface excess: there is no anomaly at high surface coverages because of anisotropic chain distributions.[62]

5.2.2. Mixed Monolayers of Surfactants and Alkanes at the a/w Interface. Mixed monolayers of surfactants and alkanes at the a−w interface have been studied in some detail.[42−44] Investigations of the surfaces of pure alkanes have shown that alkanes tend to form ordered interfacial phases in contact with air, with the hydrocarbon chains oriented normal to the interface.[33,63,64] NR results for mixed monolayers of CTAB and dodecane by Lu et al.[44] showed that the area per molecule of CTAB (at the cmc) increased to 52 Å^2 in the presence of the alkane from 43 Å^2 in the absence of the alkane and that the thickness of the hydrocarbon region of the surfactant also increased, which was interpreted in terms of a more upright conformation of the hydrocarbon chains. The *combined* surface concentration of the alkane and surfactant ($\Gamma = 5.67 \times 10^{-6}$ mol m^{-2}) was 47% higher combined than for the pure surfactant alone ($\Gamma = 3.86 \times 10^{-6}$ mol m^{-2}). If one assumes that the interfacial density is similar to that of bulk oil (or, in the terminology used in NR, the volume fraction is unity) then an increase in the combined surface excess is a prerequisite for an upright conformation, since oil is required to "fill in the gaps" between the CTAB molecules. Ellipsometry and SFS of mixed monolayers of tetradecane and CTAB at the a−w interface show a first-order phase transition (as the temperature is lowered) to a conformationally ordered state in which the d^+ mode loses all its intensity (i.e., an all-trans conformation) and the chains are oriented along the surface normal.[42] This phase has similar characteristics to the ordered monolayer formed at the interface between many alkanes and air at temperatures just above the bulk melting point of the alkane.[33,63,64] While we have no evidence for the existence of a similar phase transition at the aqueous CTAB-hexadecane interface, the fluid phase appears to adopt some of the features of the condensed phase at the a−w interface, with a preferred orientation normal to the interfacial plane.

5.2.3. Surfactant Monolayers at the CCl_4−Water Interface. Richmond and co-workers have employed SFS to study an extensive range of surfactants at the CCl_4−water interface,[39,65] including both simple single-chained ionic surfactants and phospholipids. The general trend of a decreasing ratio S_{d+}/S_{r+} with increasing bulk concentration was observed for simple ionic surfactants at the CCl_4−water interface, in agreement with the data presented here for the alkane−water interface. The closest comparison with CTAB in Richmond's work in terms of molecular structure is dodecyltrimethylammonium chloride (DTAC).[39d] The SF spectrum of DTAC at its limiting coverage is similar to our spectrum 10d, with a ratio S_{d+}/S_{r+} significantly higher than the limiting value for CTAB at the alkane−water interface. The limiting coverage measured by Richmond for DTAC is, however, only $\Gamma_{max} = 1.8 \times 10^{-6}$ mol m^{-2} which is significantly lower than $\Gamma_{max} = 2.5 \times 10^{-6}$ mol m^{-2} that we measure for CTAB. Sodium dodecyl sulfate and sodium dodecyl sulfonate had limiting surface coverages at the CCl_4−water interface similar to that of CTAB at the hexadecane−water interface[39b−d] but, surprisingly, showed a lower degree of conformational order than DTAC. The smallest value of S_{d+}/S_{r+} for simple ionic surfactants was found for dodecylammonium chloride at a limiting coverage of $\Gamma_{max} = 4.5 \times 10^{-6}$ mol m^{-2}, but even this spectrum showed more conformational disorder than we observed for CTAB at 0.6 mM. None of the surfactants studied at the CCl_4−water interface show the sharp increase in conformational order near Γ_{max} that we have observed for CTAB at the alkane−water interface. For phospholipids adsorbed at the CCl_4−water interface, a decrease in conformational order with increasing chain length was observed.[39e] Walker et al. reported that this unexpected behavior may be caused by solvation of the alkyl chains by the CCl_4, which screens chain−chain interaction and promotes chain disorder.[66] Under these circumstances, increasing the chain length leads to an increase in the number of defects,[39c] an effect not observed for monolayers of alkyl chains at interfaces without carbon tetrachloride.[66] This behavior marks an important difference between CCl_4−water and the oil−water interfaces. For example, when an alkane replaces carbon tetrachloride as the liquid in contact with a dioctadecyldimethylammonium chloride (DOAC) monolayer on quartz, the longer length alkanes (C_{14} and C_{16}) promote order in the DOAC hydrocarbon chains.[66]

5.2.4. Surfactant Monolayers at the Hydrophobic Solid−Liquid Interface. Davies and co-workers have used SFS to study the interface between a hydrophobic solid and aqueous solutions of surfactants.[67] The hydrophobic solid was a self-assembled monolayer of d_{37}-octadecanethiol on gold (dODT/Au) and, of the surfactants studied, the homologue tetradecyl trimethylammonium bromide (C_{14}TAB) is most similar to the CTAB considered here. For an aqueous solution of C_{14}TAB at the dODT/Au interface, the surfactant chains are orientated toward the hydrophobic solid and the polar headgroups toward the aqueous phase.[67a,b] A quantitative comparison of the ratio S_{d+}/S_{r+} is not possible, since the spectra from monolayers on gold contain contributions from both χ_{xxz} and χ_{zzz}. The wide range of surfactants studied at the solid−water interface, however, indicate substantial variation in conformational disorder with S_{d+}/S_{r+} ranging from 0.2 for dodecanol to 3.9 for dodecylpyridinium chloride. For C_{14}TAB near the cmc, the value of $S_{d+}/S_{r+} = 3.2$ lies near the top of this range. The absence of mixing

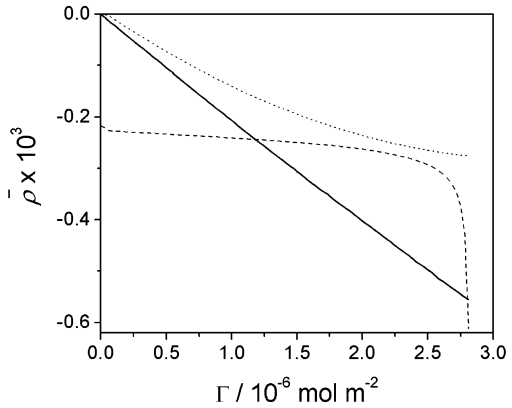

Figure 15. Contributions to $\bar{\rho}$ for a CTAB monolayer at the oil−water interface: $\bar{\rho}_{TMA}$ from the trimethylammonium headgroups (dotted line), $\bar{\rho}_{Br}$ from the bromide counterions (solid line), and $\bar{\rho}_R$ from the roughness of the interface (dashed line), all shown as a function of surface excess. $\bar{\rho}_h$ is assumed to be zero in an isotropic chain model. The sum $\bar{\rho} = \bar{\rho}_h + \bar{\rho}_{TMA} + \bar{\rho}_{Br} + \bar{\rho}_R$ is shown in Figure 14.

between the surfactant and the self-assembled monolayer militates against an upright conformation in the surfactant chains.

6. Conclusions

A new experimental approach has been developed for the acquisition of sum-frequency spectra from the bulk oil−water interface. The key features of this approach are the stabilization of a thin oil film between a sapphire prism and an aqueous phase and the use of total internal reflection to enhance the total signal and discriminate against signals from other interfaces in the system. Even with an oil film only 50-μm thick, there is significant attenuation of the IR laser within the oil and careful correction of the SF spectra is required.

With this new methodology, we have obtained the first SF vibrational spectra of surfactant monolayers at an alkane−water interface. At low concentrations, the model system of CTAB/hexadecane showed the expected features in the C−H stretching region, characteristic of a conformationally disordered monolayer. As the bulk concentration approached the cmc, the spectra changed to one characteristic of a more ordered, upright conformation. Ellipsometric measurements supported this conclusion. This qualitative structural change is not observed in analogous monolayers at the a−w interface, CCl_4−water interface, or in surfactant solutions in contact with a hydrophobic solid surface. Mixed monolayers of CTAB and alkanes at the a−w interface do have a propensity to form ordered upright phases (as do pure alkanes at their interface with air[63a,68]). This propensity is reflected in a more upright orientation in the fluid interfacial phases studied in this paper.

This paper begins to address the question of how the structure of surfactant monolayers at the oil−water differs from that at the air−water or solid−water interface and points to the importance of mixing of the oil and surfactant in determining the structure. Clearly, these studies will need to be extended to a range of other surfactants and oils to build a complete picture, but our work does signpost the road ahead. The methodology we describe is generally applicable to surfactants (even those with appreciable solubility in the oil phase) and to various oils, provided that one or other can be obtained in deuterated form. Certain refinements to the methodology would be desirable, such as effective thermostating and more durable prism coatings, perhaps through the deposition of thin silica layers onto the sapphire prism.

Acknowledgment. We thank the British Marshall Commemoration Commission for a Marshall Scholarship and the National Science Foundation for a Graduate Research Fellowship to M.M.K. We thank EPSRC and Unilever Research for funding this project in its early stages.

Appendix: Calculation of Coefficient of Ellipticity for CTAB Monolayers at the o−w Interface

We divide the contribution of the interface to $\bar{\rho}$ into four terms arising from the hydrocarbon chains, the TMA headgroups, the Br^- counterions, and the roughness of the interface. We then have

$$\bar{\rho} = \bar{\rho}_h + \bar{\rho}_{TMA} + \bar{\rho}_{Br} + \bar{\rho}_R \tag{A1}$$

The evaluation of the contribution $\bar{\rho}_h$ from the hydrocarbon chains is described in the main text. To calculate $\bar{\rho}_{TMA}$, we first estimate the intrinsic dielectric constant of TMA groups from the Clausius−Mossotti relationship

$$\frac{\epsilon - 1}{\epsilon + 2} = \frac{R_m}{V_m} \tag{A2}$$

where the molar refractivity $R_m = 20.05$ cm^3 mol^{-1} can be calculated from tabulated values of bond refractivities[69] and the molar volume of $N(CH_3)_3Br$ has been taken to be 140 Å^3[,70] from which the molar volume of Br^- (32 Å^3) is subtracted.

We next assume that the TMA headgroups are hydrated and form a mixed layer of TMA groups and water with a thickness of 8 Å—a value estimated from neutron scattering profiles.[70] The dielectric constant of this layer is obtained from the Lorentz−Lorenz effective medium approximation (the choice of EMA has a minimal effect on the results):

$$\frac{\epsilon - 1}{\epsilon + 2} = \varphi_{water}\left(\frac{\epsilon_{water} - 1}{\epsilon_{water} + 2}\right) + \varphi_{TMA}\left(\frac{\epsilon_{TMA} - 1}{\epsilon_{TMA} + 2}\right) \tag{A3}$$

where the volume fractions ϕ_{water} and ϕ_{TMA} are determined from the surface excess of CTAB and the molar volume of TMA. The contribution of the TMA groups to the ellipsometric thickness is given by the isotropic version of the Drude equation (eq 15):

$$\eta = \frac{(\epsilon - \epsilon_1)(\epsilon - \epsilon_2)}{\epsilon} d \tag{A4}$$

and $\bar{\rho}_{TMA}$ is then given by eq 14.

The counterion contribution $\bar{\rho}_{Br}$ could be calculated in an analogous manner to the headgroup contribution or alternatively one can treat the counterions as being uniformly distributed over a depth of solvent equal to the Debye length and then use tabulated values of the refractive index, n, of KBr solutions[71] as a function of concentration to determine the value of ϵ to substitute in eq A4. (The contribution of K^+ to n can be neglected because of the small size and polarizability of the K^+ ion.) By either method, $\bar{\rho}_{Br}$ is a linear function of Γ and the slope is independent of the precise value chosen for the Debye length.

The roughness contribution $\bar{\rho}_R$ arises from scattering by capillary waves and can be evaluated from capillary wave theory:[58]

$$\bar{\rho}_R = -\frac{3\pi(\epsilon_1 - \epsilon_2)}{2\lambda(\epsilon_1 + \epsilon_2)^{3/2}}\sqrt{\frac{\pi kT}{6\sigma}} \tag{A5}$$

where σ is the interfacial tension. For the oil−water interface, $\bar{\rho}_R$ is negative and a highly nonlinear function of Γ. These three contributions to $\bar{\rho}$ are shown in Figure 15 and their sum is shown in Figure 14.

References and Notes

(1) (a) Walstra, P.; Deroos, A. L. *Food Rev. Int.* **1993**, *9*, 503. (b) Krog, N. *ACS Symposium Ser.* **1991**, *448*, 138. (c) Taylor, J. A. G.; Mingis, J.; Pethica, B. A.; Yan, B. Y. J.; Jackson, C. M. *Biochim. Biophys. Acta* **1973**, *323*, 157.

(2) Harwell, J. H.; Sabatini, D. A.; Knox, R. C. *Colloids Surf. A* **1999**, *151*, 255.

(3) (a) Manning-Benson, S.; Bain, C. D.; Darton, R. C. *J. Colloid Interface Sci.* **1997**, *189*, 109. (b) Manning-Benson, S.; Bain, C. D.; Darton, R. C.; Sharpe, D.; Eastoe, J.; Reynolds, P. *Langmuir* **1997**, *13(22)*, 5808. (c) Manning-Benson, S.; Parker, S. R. W.; Bain, C. D. *Langmuir* **1998**, *14(5)*, 990.

(4) Knock, M. M.; Bain, C. D. *Langmuir* **2000**, *16*, 2857.

(5) (a) Bell, G. R.; Manning-Benson, S.; Bain, C. D. *J. Phys. Chem. B* **1998**, *102*, 218. (b) Casson, B. D.; Bain, C. D. *J. Phys. Chem. B* **1999**, *103(22)*, 4678.

(6) Lu, J. R.; Thomas, R. K.; Binks, B. P.; Fletcher, P. D. I.; Penfold, J. *J. Phys. Chem.* **1995**, *99*, 4113.

(7) (a) Adamczyk, Z.; Para, G.; Warszynski, P. *Langmuir* **1999**, *15*, 8383. (b) Velegol, S. B.; Fleming, B. D.; Biggs, S.; Wanless, E. J.; Tilton, R. D. *Langmuir* **2000**, *16*, 2548.

(8) Rosen, Milton J. *Surfactants and Interfacial Phenomena*, 2nd ed.; John Wiley and Sons: New York, 1989.

(9) Buff, F. P.; Lovett, R. A.; Stillinger, F. H. *Phys. Rev. Lett.* **1965**, *15*, 621.

(10) Goebel, A.; Lunkenheimer, K. *Langmuir* **1997**, *13*, 369.

(11) (a) Cosgrove, T.; Phipps, J. S.; Richardson, R. M. *Colloids Surf.* **1992**, *62*, 199. (b) Cosgrove, T.; Phipps, J. S.; Richardson, R. M. *Langmuir* **1994**, *9*, 3530.

(12) Staples, E.; Penfold, J.; Tucker, I. *J. Phys. Chem. B* **2000**, *104*, 606.

(13) Bowers, J.; Zarbakhsh, A. *Langmuir* **2001**, *17*, 140.

(14) Schlossman, M. L. *Curr. Opin. Colloid Interface Sci.* **2002**, *7*, 235.

(15) Fradin, C.; Luzet, A.; Braslau, A.; Alba, M.; Muller, F.; Daillant, J. *Langmuir* **1998**, *14*, 7327.

(16) Mitrinovic, D. M.; Zhang, Z.; Williams, S. M.; Huang, Z.; Schlossman, M. L. *J. Phys. Chem. B* **1999**, *11*, 1779.

(17) Tikhonov, A. M.; Li, M.; Schlossman, M. L. *J. Phys. Chem. B* **2001**, *105(34)*, 8065.

(18) Uredat, S.; Findenegg, G. H. *Langmuir* **1999**, *15*, 1108.

(19) Piasecki, D. A.; Wirth, M. J. *J. Phys. Chem.* **1993**, *97*, 7700.

(20) Sassaman, J. L.; Wirth, M. J. *Colloids Surf., A* **1994**, *93*, 49.

(21) Gajraj, A.; Ofoli, R. Y. *Langmuir* **2000**, *16*, 4279.

(22) Tupy, M. J.; Blanch, H. W.; Radke, C. J. *Ind. Eng. Chem. Res.* **1998**, *37*, 3159.

(23) Keddie, J. L. *Curr. Opin. Colloid Interface Sci.* **2001**, *6*, 102.

(24) (a) de Hoog, E. H. A.; Lekkerkerker, H. N. W.; Schulz, J.; Findenegg, G. H. *J. Phys. Chem. B* **1999**, *103*, 10657. (b) Schultz, J.; Hirtz, A.; Findenegg, G. H. *Physica A* **1997**, *244*, 334.

(25) Russev, S. C.; Arguirov, T. V.; Gurkov, T. D. *Colloids Surf., B* **2000**, *19*, 89.

(26) Beaglehole, D.; Lawson, F.; Harper, G.; Hossain, M. *J. Colloid Interface Sci.* **1997**, *192*, 266.

(27) Bloembergen, N. *Appl. Phys. B* **1999**, *68*, 289.

(28) (a) Shen, Y. R. *Surf. Sci.* **1994**, *299/300*, 551. (b) Corn, R. M.; Higgins, D. A. *Chem. Rev.* **1994**, *94*, 107.

(29) Wang, H. F.; Borguet, E.; Eisenthal, K. B. *J. Phys. Chem. A* **1997**, *101*, 713.

(30) Tamburello-Luca, A. A.; Hebert, P.; Antoine, R.; Brevet, P. F.; Girault, H. H. *Langmuir* **1997**, *13*, 4428.

(31) Grubb, S. G.; Kim, M. W.; Rasing, T.; Shen, Y. R. *Langmuir* **1988**, *4*, 452.

(32) Tamburello-Luca, A. A.; Hebert, P.; Brevet, P. F.; Girault, H. H. *J. Chem. Soc., Faraday Trans.* **1996**, *92*, 3079.

(33) Conboy, J. C.; Daschbach, J. L.; Richmond, G. L. *J. Phys. Chem.* **1994**, *98*, 9688.

(34) (a) Naujok, R. R.; Paul, H. J.; Corn, R. M. *J. Phys. Chem.* **1996**, *100(25)*, 10498. (b) Paul, H. J.; Corn, R. M. *J. Phys. Chem. B* **1997**, *101*, 4494.

(35) (a) Hunt, J. H.; Guyot-Sionnest, P.; Shen, Y. R. *Chem. Phys. Lett.* **1987**, *133*, 189. (b) Shen, Y. R. *Nature* **1989**, *333*, 519.

(36) (a) Ong, T. H.; Davies, P. B.; Bain, C. D. *Langmuir* **1993**, *9*, 1836. (b) Braun, R.; Casson, B. D.; Bain, C. D.; van der Ham, E. W. M.; Vrehen, Q. H. F.; Eliel, E. R.; Briggs, A. M.; Davies, P. B. *J. Chem. Phys.* **1999**, *110(9)*, 4634. (c) Williams, C. T.; Yang, Y.; Bain, C. D. *Langmuir* **2000**, *16(5)*, 2343.

(37) Bain, C. D. *J. Chem. Soc., Faraday Trans.* **1995**, *91(9)*, 1281.

(38) (a) Bell, G. R.; Bain, C. D.; Ward, R. N. *J. Chem. Soc., Faraday Trans.* **1996**, *92(4)*, 515. (b) Bell, G. R.; Manning-Benson, S.; Bain, C. D. *J. Phys. Chem. B* **1998**, *102*, 218. (c) Bell, G. R.; Li, Z. X.; Bain, C. D.; Fischer, P.; Duffy, D. C. *J. Phys. Chem. B* **1998**, *102*, 9461. (d) Goates, S. R.; Schofield, D. A.; Bain, C. D. *Langmuir* **1999**, *15(4)*, 1400.

(39) (a) Messmer, M. C.; Conboy, J. C.; Richmond, G. L. *J. Am. Chem. Soc.* **1995**, *117*, 8039. (b) Conboy, J. C.; Messmer, M. C.; Richmond, G. L. *J. Phys. Chem.* **1996**, *100*, 7617. (c) Conboy, J. C.; Messmer, M. C.; Richmond, G. L. *Langmuir* **1998**, *14*, 6722. (d) Conboy, J. C.; Messmer, M. C.; Richmond, G. L. *J. Phys. Chem. B* **1997**, *101*, 6724. (e) Walker, R. A.; Conboy, J. C.; Richmond, G. L. *Langmuir* **1997**, *13*, 3070.

(40) Du, Q.; Freysz, E.; Shen, Y. R. *Science* **1994**, *264*, 826.

(41) Brochard-Wyart, F.; Di Meglio, J. M.; Quéré, D.; De Gennes, P. G. *Langmuir* **1991**, *7*, 335.

(42) (a) Lei, Q.; Bain, C. D. unpublished results. (b) McKenna, C. E.; Knock, M. M.; Bain, C. D. *Langmuir* **2000**, *16*, 5853.

(43) Lu, J. R.; Thomas, R. K.; Aveyard, R.; Binks, B. P.; Cooper, P.; Fletcher, P. D. I.; Sokolowski, A.; Penfold, J. *J. Phys. Chem.* **1992**, *96*, 10971.

(44) Lu, J. R.; Thomas, R. K.; Binks, B. P.; Fletcher, P. D. I.; Penfold, J. *J. Phys. Chem.* **1995**, *99*, 4113.

(45) (a) Lu, J. R.; Thomas, Li, Z. X.; Thomas, R. K.; Binks, B. P.; Crichton, D.; Fletcher, P. D. I.; McNab, J. R.; Penfold, J. *J. Phys. Chem. B* **1998**, *102*, 5785. (b) Binks, B. P.; Crichton, D.; Fletcher, P. D. I.; MacNab, J. R.; Li, Z. X.; Thomas, R. K.; Penfold, J. *Colloids Surf., A* **1999**, *146*, 299.

(46) Thoma, M.; Schwendler, M.; Baltes, H.; Helm, C. A.; Pfohl, T.; Riegler, H.; Möhwald, H. *Langmuir* **1996**, *12*, 1722.

(47) Lei, Q.; Bain, C. D. unpublished results.

(48) Ward, R. N.; Duffy, D. C.; Davies, P. B.; Bain, C. D. *J. Phys. Chem.* **1994**, *98*, 8536.

(49) Bigelow, W. C.; Pickett, D. L.; Zisman, W. A. *J. Colloid Sci.* **1946**, *1*, 513.

(50) Crystran Crystals, BDH Advanced Materials Division, England.

(51) Bertie, J. E.; Khalique-Ahmed, M.; Baluja, S. *J. Phys. Chem.* **1989**, *93*, 2214.

(52) Bell, G. R.; Li, Z. X.; Bain, C. D.; Fischer, P.; Duffy, D. C. *J. Phys. Chem. B* **1998**, *102*, 9463.

(53) Born, M.; Wolf, E. *Principles of Optics*, 6th ed.; Cambridge University Press: Cambridge, U.K., 1980; p 40.

(54) Bain, C. D. Evall, J.; Whitesides, G. M. *J. Am. Chem. Soc.* **1989**, *111*, 7164.

(55) MacPhail, R. A.; Strauss, H. L.; Snyder, R. G.; Elliger, C. A. *J. Phys. Chem.* **1984**, *88*, 334.

(56) (a) Szyszkowski, B. *Z. Phys. Chem.* **1908**, *64*, 385. (b) Prosser, A. J.; Franses, E. I. *Colloids Surf., A* **2001**, *178*, 1.

(57) Duffy, D. C.; Davies, P. B.; Creeth, A. M. *Langmuir* **1995**, *11*, 2931.

(58) Meunier, J. *J. Phys.* **1987**, *48*, 1819.

(59) Casson, B. D.; Bain, C. D. *Langmuir* **1997**, *13*, 5465.

(60) Lu, J. R.; Thomas, R. K.; Penfold, J. *Adv. Colloid Interface Sci.* **2000**, *84*, 143.

(61) (a) Lu, J. R.; Lee, E. M.; Thomas, R. K. *Acta Crystallogr., Sect. A* **1996**, *A52*(1), 11. (b) Lu, J. R.; Li, Z. X.; Smallwood, J.; Thomas, R. K.; Penfold, J. *J. Phys. Chem.* **1995**, *99*, 8233. (c) Lu, J. R.; Hromadova, M.; Simister, E. A.; Thomas, R. K.; Penfold, J. *J. Phys. Chem.* **1994**, *98*, 11519. (d) Lu, J. R.; Hromadova, M.; Simister, E.; Thomas, R. K.; Penfold, J. *Physica B* **1994**, *198*, 120.

(62) Manning-Benson, S.; Parker, S. R. W.; Bain, C. D.; Darton, R. C.; Penfold, J. *Langmuir* **1998**, *14*, 990.

(63) (a) Ocko, B. M.; Wu, X. Z.; Sirota, E. B.; Gang, O.; Deutsch, M. *Phys. Rev. E* **1997**, *55(3)*, 3164. (b) Colussi, A. J.; Hoffmann, M. R.; Tang, Y. *Langmuir* **2000**, *16(12)*, 5213.

(64) Birdi, K. S. *Colloids Surf., A* **1997**, *123*−*124*, 543.

(65) Richmond, G. L. *Anal. Chem. News Features* **1997**, 536A−543A.

(66) Miranda, P. B.; Shen, Y. R. *J. Phys. Chem. B* **1999**, *103*, 3292.

(67) (a) Ward, R. N.; Duffy, D. C.; Davies, P. B.; Bain, C. D. *J. Phys. Chem.* **1994**, *98* (34), 8356. (b) Ward, R. N.; Davies, P. B.; Bain, C. D. *J. Phys. Chem.* **1993**, *97*, 7141. (c) Bain, C. D. *J. Chem. Soc., Faraday Trans.* **1995**, *91(9)*, 1281.

(68) (a) Sefler, G. A.; Du, Q.; Miranda, P. B.; Shen, Y. R. *Chem. Phys. Lett.* **1995**, *235*, 347. (b) Pfohl, T.; Beaglehole, D.; Riegler, H. *Chem. Phys. Lett.* **1996**, *260*, 82.

(69) Atkins, P. W. *Physical Chemistry*, 3rd ed.; Oxford University Press: Oxford, U.K., 1986; p 582.

(70) Lu, J.; Simister, E.; Thomas, R. K. T.; Penfold, J. *J. Phys. Chem.* **1993**, *97*, 6024.

(71) Handbook of Chemistry and Physics, 64th ed.; CRC Press: Boca Raton, FL, 1983; p D-246.